Surface modification of additive manufactured components by ultrasonic cavitation abrasive finishing

Author names and affiliation

K.L. Tan[a,b], S.H. Yeo[a,b,*]

a) School of Mechanical and Aerospace Engineering, Nanyang Technological University, 50 Nanyang Avenue, Singapore 639798.

b) Rolls-Royce@NTU Corporate Lab, N3.1-B2a-01, 50 Nanyang Avenue, Singapore 639798.

*Corresponding author. Tel.: +65 6790 5539. Email address: mshyeo@ntu.edu.sg

Abstract

Powder Bed Fusion (PBF) is a group of powder-bed based layered Additive Manufacturing (AM) techniques for direct fabrication of metal and metal alloys. Despite its advancements, the surface quality of as-built PBF components remains unsatisfactory. In this paper, a new post-process finishing technique, based on ultrasonic cavitation effects in a solid-liquid mixture, is introduced for PBF-built components. Trials were conducted on side surfaces of Inconel 625 manufactured by Direct Metal Laser Sintering (DMLS). Results have demonstrated that this technique improves *Ra* values of as-built Inconel 625 side surfaces by up to 45% after 30 minutes of processing time. Scanning electron microscopic images revealed that most small-sized partially melted powders were removed through heterogeneous cavitation nucleation on the specimens' rough initial surface. A secondary fine-scale erosion mechanism by micro-abrasives, accelerated by cavitation bubble collapses, further depressed difficult-to-remove irregularities.

Keywords

Ultrasonic cavitation abrasive finishing, additive manufacturing, AM post-processing, surface modification, partially melted powders

1. Introduction

Metal-based AM techniques have witnessed development at a dramatic pace over the past two decades. Among the numerous metal-based AM methods, PBF has emerged as the industry and research standard. PBF processes include DMLS, Selective Laser Melting (SLM) and Electron Beam Melting (EBM). Their capability to fabricate components with a high-strength-to-weight ratio has captured imaginations of designers and engineers alike. Despite its vast potential, a significant disadvantage arises in the poor surface quality of PBF components. For instance, average surface roughness, *Ra*, of as-built DMLS/SLM parts is typically larger than 10 μm [1]. Poor aesthetic appearances aside, the high surface roughness of PBF components could be detrimental to their fatigue and frictional properties. Wycisk et

al. [2] have argued that surface defects on as-built SLM Ti-6Al-4V act as crack initiation sites, hence resulting in its significantly lower fatigue endurance limit. Mower and Long [3] also reported that the fatigue strengths exhibited by all four PBF-built metal alloys are considerably lower (up to 40%) than their wrought and polished counterparts.

In order to meet the stringent requirements in engineering applications, post-process finishing of PBF components is often necessary [4]. Recently, laser polishing emerged as a potential cost-effective surface finishing solution for SLM surfaces [5]; as the same PBF laser source could be used for in-process polishing [6]. Roughness improvement of over 80 % was reported [7]. While laser polishing is promising, re-melting the surface could further exacerbate the thermal residual stress or even result in undesirable change in surface chemistry [8]. Chemical polishing [9] has also been developed to finish AM porous structures. While the process is effective, it tends to erode material indiscriminately hence compromising the dimensional accuracy of the components [10].

The mechanical effects of high-intensity ultrasound have been utilised in material removal processes, such as ultrasonic machining [11] and scale deposit removal [12]. When a high frequency sinusoidal ultrasonic pressure wave is induced in a liquid medium, cavitation occurs. In this work, cavitation refers to the formation, growth and collapse of inertial cavitation bubbles. Bubble collapses produce high velocity micro-jets (200-700 m/s) when they occur within the close proximity of a specimen surface [13]. Furthermore, it has been reported that the introduction of micro-particles would alter the cavitation dynamics. Micro-particles act as bubble nucleation sites, hence increasing the overall cavitation intensity [14]. In addition, shockwaves from individual or cloud bubble collapses are thought to accelerate micro-particles to high velocity, thereby impacting and eroding the surface layer through micro-ploughing and micro-cutting mechanisms [15]. This principle has been traditionally studied as a damage mechanism, which results in surface roughness deterioration on components. To the authors' knowledge, no prior work has been conducted to develop this principle into a surface modification or finishing technique.

In this study, surface improvement of DMLS-built Inconel 625 specimens will be demonstrated using the developed process. Due to the addition of micro-abrasives in this process, this technique is termed as Ultrasonic Cavitation Abrasive Finishing (UCAF) by the authors. According to scanning electron microscopic images and surface topography studies, the roughness improvement mechanisms will be proposed and discussed.

2. Methods

2.1 Work material

The base material used in this study is Inconel 625 manufactured by DMLS (EOS M290, EOS GmbH). The metal powder size ranges between 10 to 55 µm, with its composition outlined Table 1. This material was selected as it is a heat and corrosion resistant material widely deployed in industries, such as aerospace. Representative cubic specimens (20 mm × 20 mm × 20 mm) were built with the recommended parameters by the manufacturer. Optimal

parameters for up-skin, in-skin and down-skin building were deployed, in addition to contouring strategies. The specimens were then wire-cut from the build plate, annealed at 870 ˚C for 1 hour and cleaned in an ultrasonic cleaner for 15 minutes to remove loosely-attached powder. The build orientation and target finishing surfaces (side surfaces) are illustrated in Fig. 1. The side surfaces are selected for this preliminary study due to their unique surface texture dominated by partially melted powders.

Table 1 EOS Inconel 625 powder composition.

Element	Ni	Cr	Mo	Nb	Fe	Ti	Al	Co	C	Ta	Si	Mn	P	S
Wt %	Balance	20-23	8-10	3.15-4.15	≤ 5	≤ 0.4	≤ 0.4	≤ 1	≤ 0.1	≤ 0.05	≤ 0.5	≤ 0.5	≤ 0.015	≤ 0.015

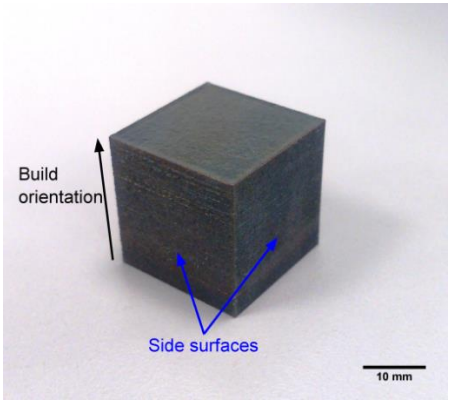

Fig. 1. DMLS Inconel specimen.

2.2 UCAF setup

Ultrasonic wave of 20 kHz frequency was generated by a high-power ultrasonic generator (Q700, Qsonica Llc) and transmitted over the transducer and horn assembly to reach peak-to-peak vibration amplitude of 60 µm at horn tip. The diameter of the horn tip used in this study is 12.7 mm. Specimens were held with a fixture and immersed in a container filled with abrasive slurry, with the target finishing surface facing upwards. Abrasive slurry consists of SiC micro-particles, a type of commonly-used hard abrasives, of 400, 800 and 1200 grit sizes (of 22.5, 12 and 5.5 µm respectively) in deionised water. The experimental conditions in this study are listed in Table 2. In order to study the role of micro-abrasives in this process, a benchmark without the addition of abrasive particles (pure cavitation effects) is established. For the rest of the trials, a moderate 5 wt% abrasive concentration was used to enhance cavitation effects effectively. The horn tip was positioned at approximately 0.8 mm away from the specimen surface to avoid contact between the two. In addition, this working gap is sufficient to prevent direct hammering of abrasive particles (max peak-to-peak amplitude of 60 µm vs max average abrasive size of 23 µm) during the process. During UCAF, abrasive slurry was recirculated by a peristaltic pump (323D, Watson Marlow) to ensure that there was a constant supply of fresh abrasive particles to the finishing zone. An ultrasonic duty cycle of 50% was used to prevent excessive heat generation during the process. In addition, a recirculating chiller was used to regulate the temperature rise to within 2 ˚C.

Table 2 Experimental conditions.

Specimen #	Abrasive size (grit)	Abrasive Conc. (wt %)	Ultrasonic amplitude (μm)
1	No abrasive	No abrasive	60
2	1200	5	60
3	800	5	60
4	400	5	60

2.3 Material characterisation

Surface roughness measurements were then taken using a portable stylus profilometer (SJ-301, Mitutoyo). For each sample, 10 measurements were taken due to the high standard deviations. The cut-off length used was 2.5 mm. 3D topographic measurements were taken with a contact stylus profilometer (Talyscan 150, Taylor Hobson). After UCAF, the specimens were cleaned again in the ultrasonic cleaner for 15 minutes to remove abrasive particles left over on the surface. Surfaces were also observed under a scanning electron microscope (JSM5600LV, Jeol) before and at the end of each experimental run.

3. Results & Discussions

3.1 Surface quality

The target finishing surfaces, built at 90˚ sloping angle, were selected for this preliminary study due to their unique surface characteristics. Fig. 2a shows the typical side surface characteristics of as-manufactured DMLS samples. In general, the surface irregularities can be classified into 3 categories. Firstly, numerous small, almost spherical, particles were observed on the surface. As the sizes of these irregularities correspond to the EOS Inconel 625 powder size distribution (10 – 55 μm), these are observed to be the partially melted powders. During the DMLS process, surrounding powders within the powder bed were partially melted onto the surface due to heat diffusion at the layer edge [16]. Secondly, there were numerous irregularly-shaped surface peaks with significantly larger dimensions (>60 μm). These were formed due to the agglomeration of several partially melted powders or the balling phenomenon. In particular, these structures were found predominantly at the inter-layer bonding region. Lastly, despite the high machine resolution, small ‘step’ discontinuities could still be observed at the interface between neighbouring layers. Together, these contribute to the high initial *Ra* values of side surfaces.

For all experimental runs, a significant alteration of the surface by UCAF has been observed. The most noticeable topographic alteration after UCAF is the removal of partially melted powders from the surface. Fig. 2b shows the SEM image of specimen #3 after 30 minutes of UCAF, taken at the exact same area as Fig. 2a. Almost all small-sized partially melted powders were removed, leaving a flat surface without visible traces. On the other hand, larger-sized balls and irregular surface structures were more challenging to be removed. Some discontinuities present at the layers’ interface were still observed after 30 minutes of processing time. Overall, the surface modification induced by UCAF resulted in a visibly

smoother surface. The improvement in surface topography is further illustrated in the comparison of 3D topographic maps before and after UCAF (Fig. 3).

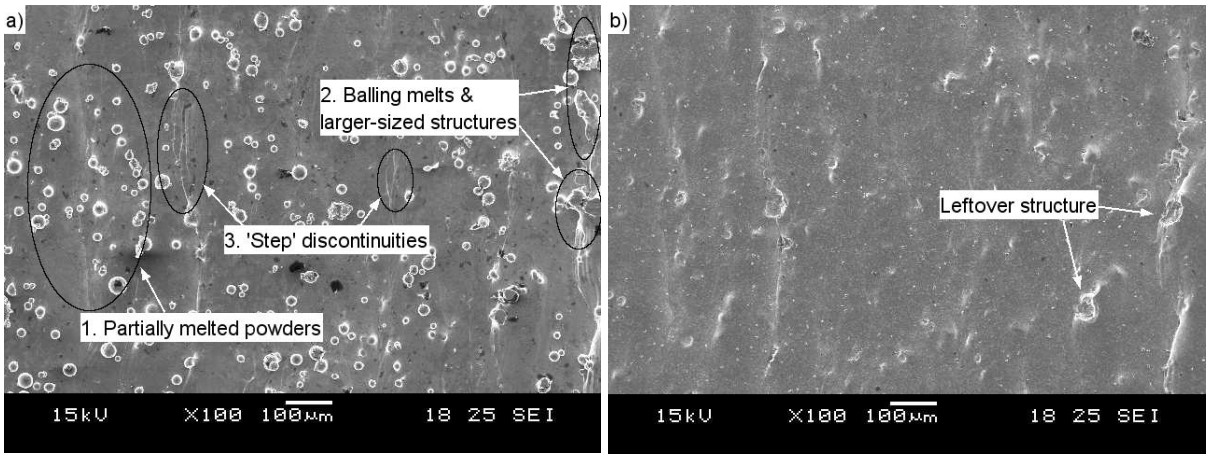

Fig. 2a. Typical side surface characteristics of as-manufactured DMLS Inconel 625 components. b. surface topography ater 30 mins of UCAF processing.

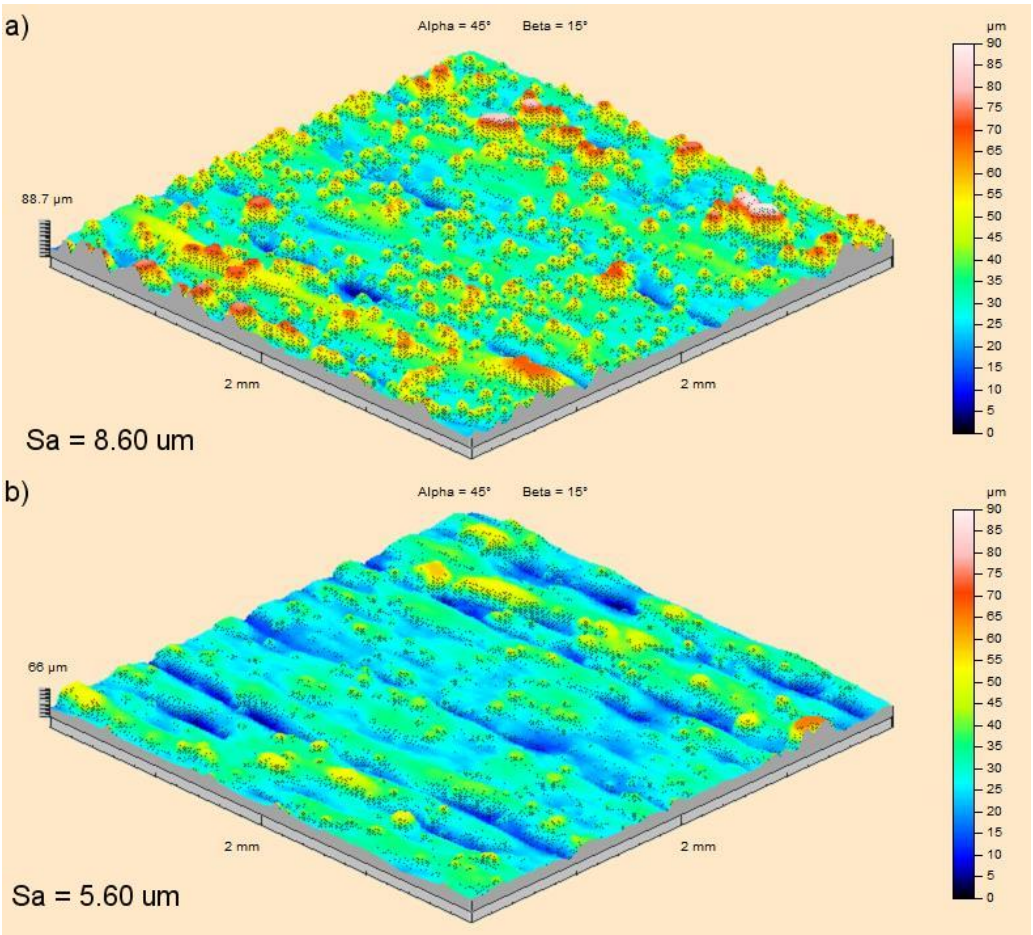

Fig. 3. Surface topography map of as-manufactured DMLS specimen. b. surface topography after 30 mins showing removals of surface peaks. (Note: the colour scale is the same for both images)

3.2 Mechanisms of material removal

Based on SEM observations, UCAF's mechanisms of material removal that led to surface roughness improvements are proposed in Fig. 4. Firstly, the mechanism behind the extensive removal of spherical partially melted powders is of particular interest. In all experimental conditions, most of the partially melted powders were removed, regardless of whether micro-abrasives were added. Hence, the removal of partially melted powders is considered to be based on pure cavitation effects. Considering the specimens' rough initial surface topography, the dominant mechanism is postulated to be heterogeneous cavitation on the specimen surface. Rough surfaces contain many crevices (e.g. the bonding neck between a partially melted powder and a surface) that could entrap gas and act as bubble nucleation sites. Cavitation bubbles nucleate and grow from the crevices; then collapse over the positive pressure cycle. Repeated impacts from the bubbles' collapses directed at the partially melted powders would ultimately dislodge them from the surface.

On the other hand, the second mechanism is related to the addition of micro-abrasives in the UCAF process. Besides enhancing cavitation phenomenon [14], [17], micro-abrasives, of the sizes investigated in this study (5.5, 12, 22.5 µm), are accelerated by shockwave emitted from cavitation bubble collapses [18]. This is verified by the observation of extensive micro-ploughing and micro-cutting marks (1 - 5 µm) on all specimen surfaces (Fig. 5). The surface texture of specimens after UCAF is similar to those observed after micro-abrasive blasting processes [19]. This mechanism aids in depressing larger-sized balls and surface peaks, resulting in an overall smoother surface.

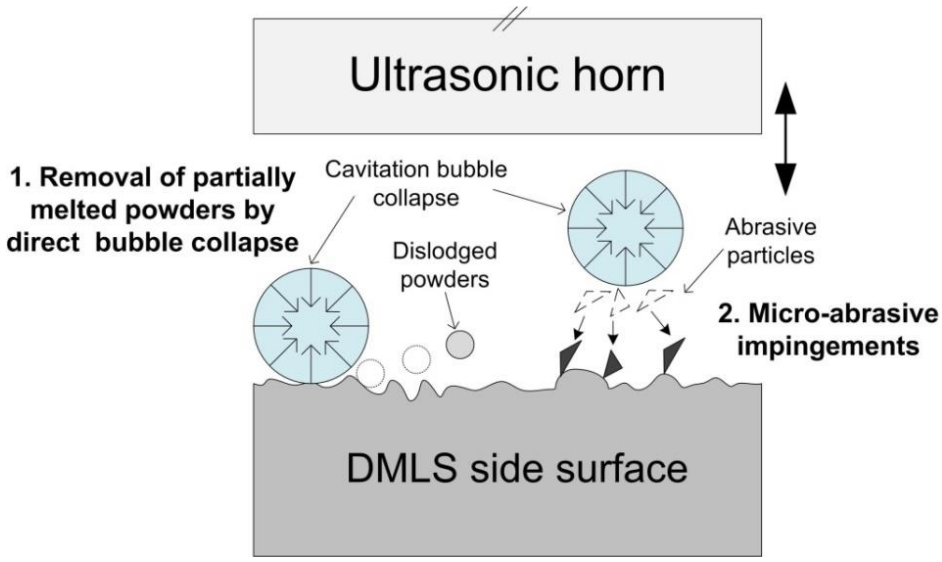

Fig. 4. Surface roughness improvement mechanisms on DMLS side surface by UCAF.

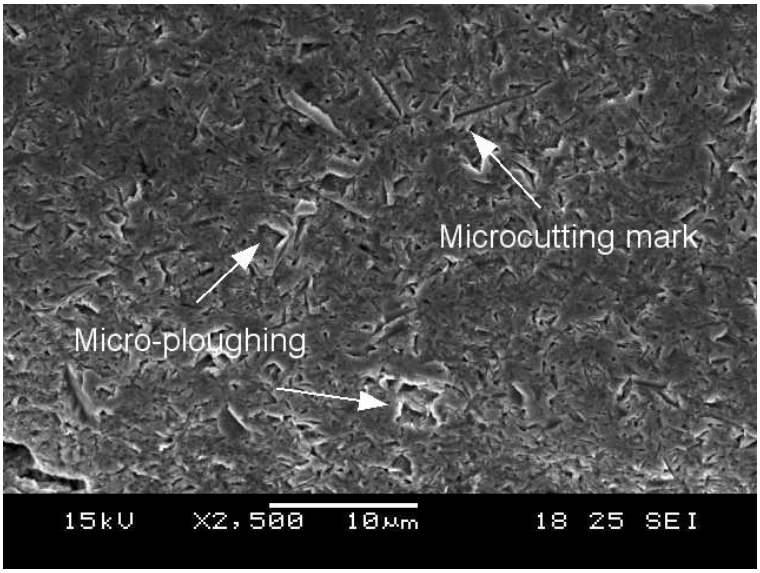

Fig. 5. SEM image showing the typical surface texture after UCAF.

3.3 Surface roughness

Fig. 6 shows the changes in average surface roughness, *Ra*, over 30 minutes for all experimental conditions. The error bars represent the standard deviations of the measurements. The initial *Ra* values of the specimens were in the range of 6.5 – 7.5 µm. *Ra* values of DMLS components improved significantly during the first 5 minutes in all runs, after which they improved gradually until the final roughness values were reached. The best final *Ra* achieved is 3.65 µm on specimen #2. To assess the efficiency of roughness improvement, percentage of *Ra* improvement is also used. In general, the roughness improvement is more substantial with the addition of abrasive particles. The best *%Ra* improvement was obtained on specimen #2 (44.3%), while the worst roughness improvement was registered on specimen #1 (30.1%). The addition of 1200 grit micro-abrasive particles leads to the best final surface finish. Given the same concentration used, the total number of abrasive particles for a smaller average abrasive size (5.5 µm) will be significantly more than the other two sizes. As micro-abrasives act as bubble nucleation sites, more particles could lead to an overall rise in cavitation intensity hence surface finishing effects.

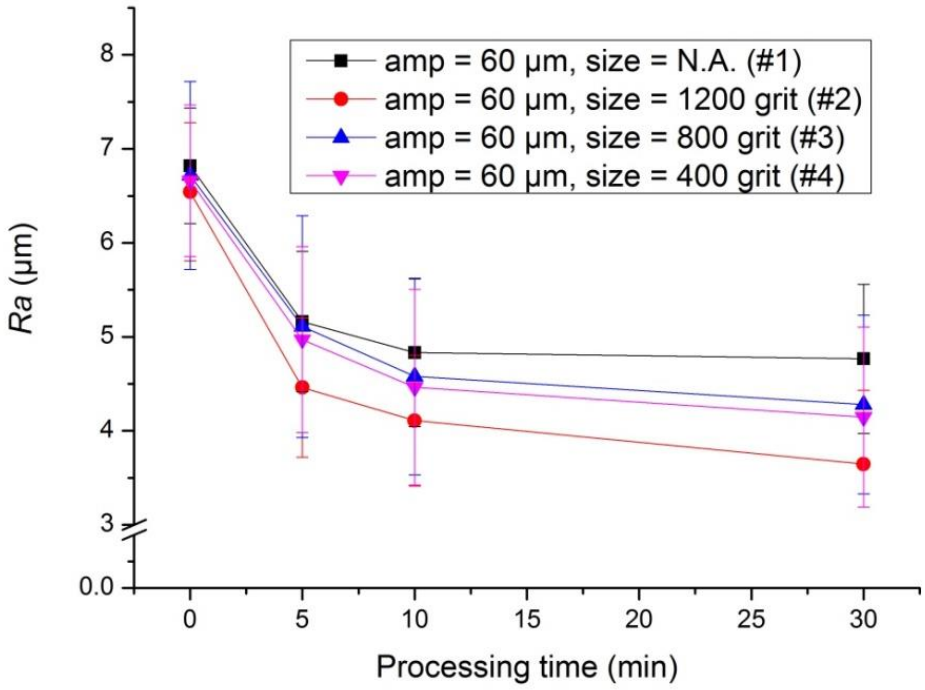

Fig. 6. *Ra* changes on DMLS side surface over processing time.

4. Discussions

In this section, the individual roles of the two mechanisms of material removal are further discussed. A closer examination of the surface characteristic after processing allows us to understand the individual mechanisms further. The first mechanism - removal of partially melted structures by direct bubble collapses – usually results in the complete removal of powders/structures (Fig. 7a). The remaining surface is characterised by a leftover crater with fatigue striation marks. On the other hand, the second mechanism – high-velocity impacts by micro-abrasives – results in the gradual erosion of surface peaks over processing time (Fig. 7b). This mechanism was only observed on specimen #2 - #4, whereby micro-abrasives were added. Surface peaks were preferentially impacted and eroded by micro-abrasives due to their relative proximity to the ultrasonic horn. This mechanism also dominates when the surface structures are fully melted onto the specimen surface; hence do not have significant 'weak spots' for bubbles to nucleate. Hence, removal by mechanism 1 is not possible.

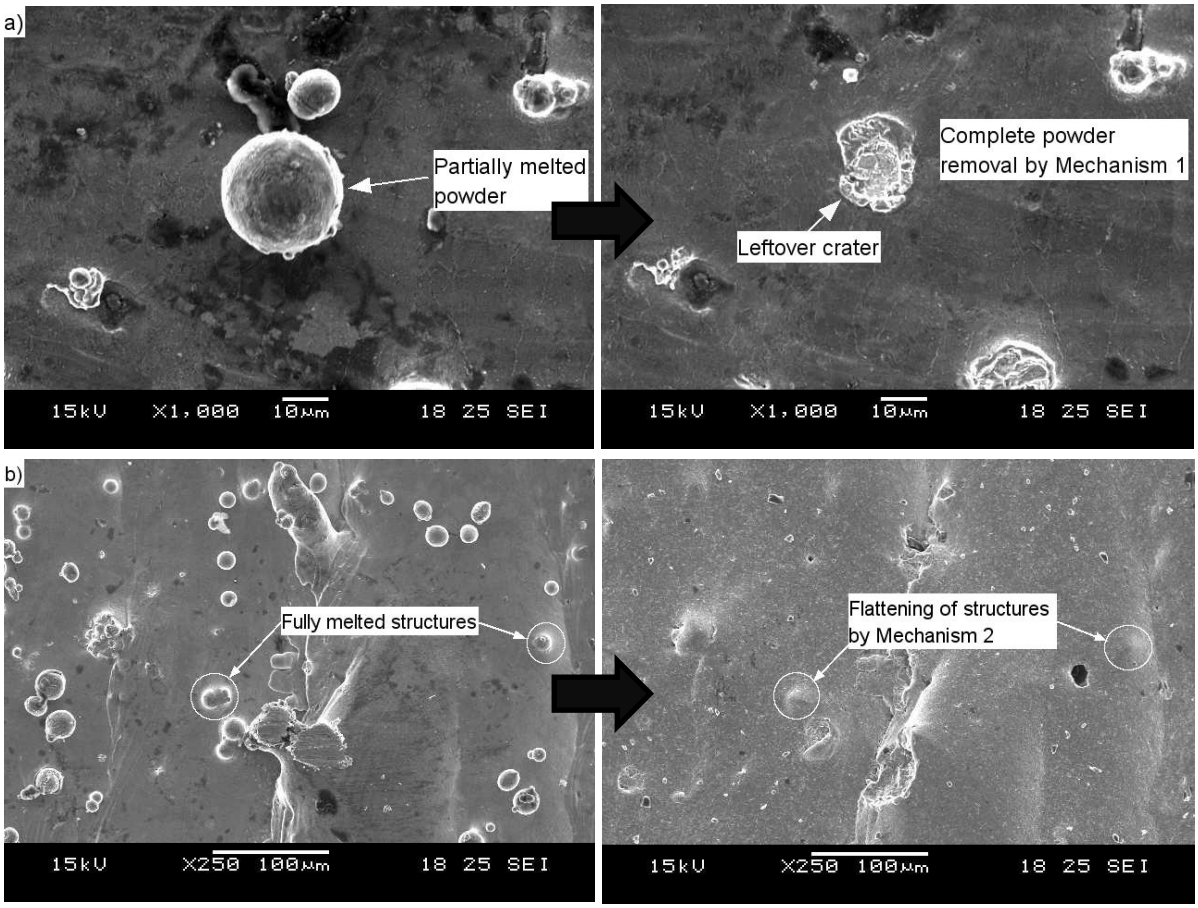

Fig. 7a. Removal phenomenon by Mechanism 1. b. fine-scale erosion of fully-melted powder/surface structures by micro-abrasive impacts

Fig. 8a—d shows the evolution of a specimen surface (#3) at various processing time intervals. During the first 5 minutes, most spherical partially melted powders with weak bonds to the surface were removed through mechanism 1. Despite this, some larger-sized balling melts and fully-melted structures remained on the surface (Fig. 8b). The subsequent 5 minutes resulted in more removals of larger-sized structures through mechanism 1, as evidenced by the removal sites observed (Fig. 8c). From 10 to 30 minutes, material removal by mechanism 1 is diminishing. This is due to the lack of crevices and discontinuities on the relatively smooth surface for bubbles to nucleate from. Any material removal during this stage was dominated by micro-abrasive impacts. Besides continuing to depress fully-melted surface structures, there was another interesting observation with regards to mechanism 2. Removal sites from prior powder/structure removal have become more homogeneous after exposure to micro-abrasive impingements.

The abovementioned observations from SEM images also explain the roughness improvement trend (Fig. 6). The surface morphology changes, hence roughness improvement, are the most significant during the first 5 minutes. After which, the roughness improvement diminishes over time. However, the roughness improvement continues even after 10 minutes for all UCAF conditions with micro-abrasives (#2 - #4). As a comparison, *Ra* values of specimen #1 (no micro-abrasives) does not improve further after the first 10 minutes. To summarise the above discussions, mechanism 1 accounts for most material removal hence roughness improvements in the UCAF process. Although mechanism 2 does not remove

material significantly, it is crucial as it aids in surface homogenisation and further roughness improvements beyond the initial stage.

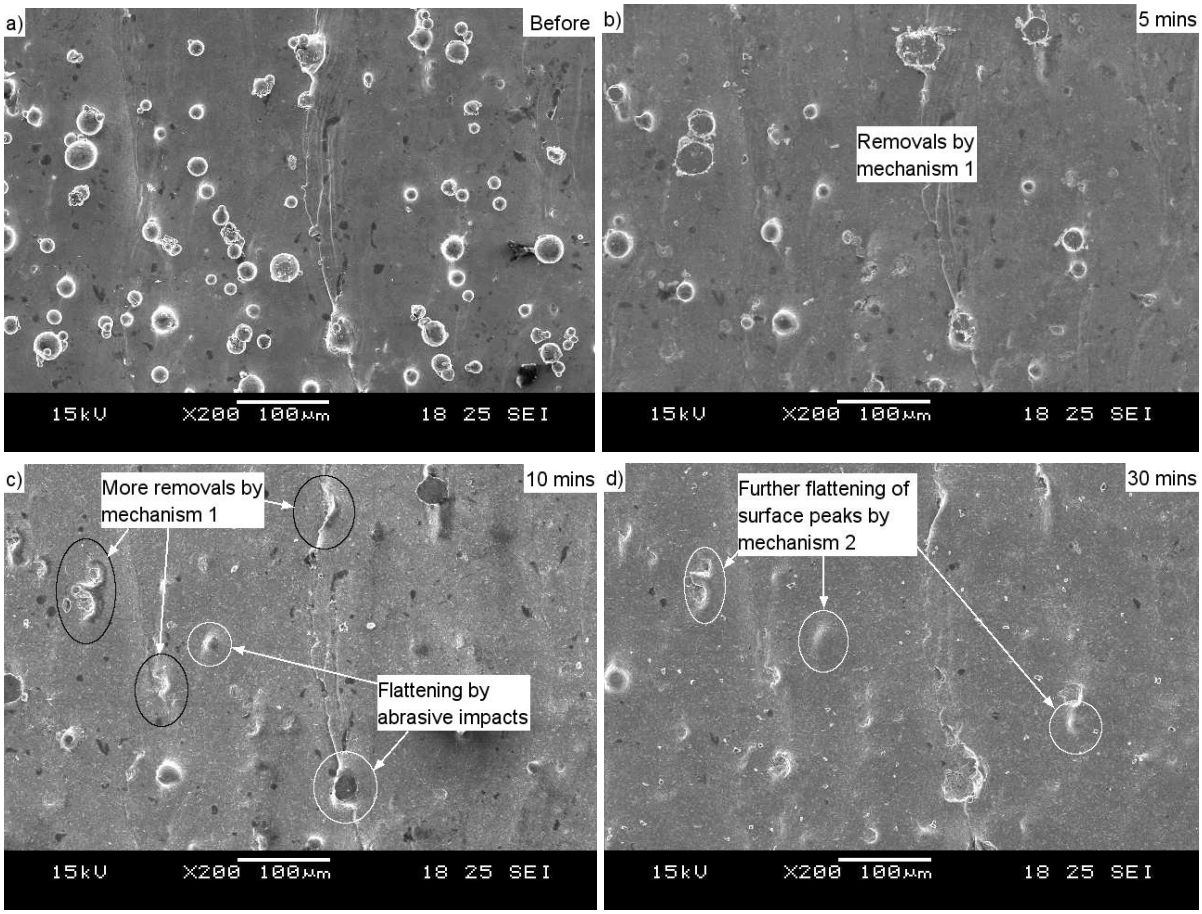

Fig. 8. Surface topography of specimen #3 a. before UCAF. b. after 5 mins of UCAF. c. after 10 minutes of UCAF. d. after 30 minutes of UCAF. (Note: All images taken at the exact same area)

Based on the above findings, UCAF could be ideal for certain engineering applications. For instance, fins manufactured by DMLS have been shown to exhibit a significantly higher convective heat transfer coefficient due to its high surface roughness [20]. However, if used as-manufactured, partially melted powders present on these surfaces could lead to flow contamination. UCAF ensures that surfaces are free from partially melted powders; while retaining the unique AM surface texture for functional purposes. For components that require a high-precision finish, UCAF could assist in bringing down the roughness from very high values to reasonable values, before fine finishing operations are carried out.

5. Conclusions

To date, cavitation effects are often associated with damage and surface roughness deterioration on smooth specimens. The preliminary findings presented in this paper suggest that components with poor surface integrity and high surface roughness could act as self-nucleating surfaces when subjected to cavitation. As a result, surface irregularities could be removed. The addition of micro-abrasives in UCAF further resulted in gradual erosion of larger-sized surface peaks and homogenising of surface texture through high-velocity abrasive impacts. Overall, side surface roughness improvements of up to 45% were recorded

on DMLS specimens through UCAF after 30 minutes. This process's potential to remove surface irregularities efficiently without extensive alteration of the original DMLS surface has distinguished it from existing post-process surface finishing techniques. Future work to be conducted includes a full parametric study of the UCAF process and an extension of its application to freeform surfaces of AM components.

Acknowledgement

This work was conducted within the Rolls-Royce@NTU Corporate Lab with support from the National Research Foundation (NRF) Singapore under the Corp Lab@University Scheme.

References

[1] D. D. Gu, W. Meiners, K. Wissenbach, and R. Poprawe, "Laser additive manufacturing of metallic components: materials, processes and mechanisms," *International Materials Reviews*, vol. 57, no. 3, pp. 133–164, 2012.

[2] E. Wycisk, A. Solbach, S. Siddique, D. Herzog, F. Walther, and C. Emmelmann, "Effects of defects in laser additive manufactured Ti-6Al-4V on fatigue properties," *Physics Procedia*, vol. 56, no. C, pp. 371–378, 2014.

[3] T. M. Mower and M. J. Long, "Mechanical behavior of additive manufactured, powder-bed laser-fused materials," *Materials Science and Engineering A*, vol. 651, pp. 198–213, 2016.

[4] E. Gordon, A. S. Chaharsooghi, and J. Flynn, "A Surface Modification Decision Tree to Influence Design in Additive Manufacturing," in *Sustainable Design and Manufacturing*, 2016, pp. 423–434.

[5] S. Marimuthu, A. Triantaphyllou, M. Antar, D. Wimpenny, H. Morton, and M. Beard, "Laser polishing of selective laser melted components," *International Journal of Machine Tools and Manufacture*, vol. 95, pp. 97–104, 2015.

[6] E. Yasa, J.-P. Kruth, and J. Deckers, "Manufacturing by combining Selective Laser Melting and Selective Laser Erosion/laser re-melting," *CIRP Annals - Manufacturing Technology*, vol. 60, no. 1, pp. 263–266, 2011.

[7] A. Lamikiz, J. A. Sánchez, L. N. López de Lacalle, and J. L. Arana, "Laser polishing of parts built up by selective laser sintering," *International Journal of Machine Tools and Manufacture*, vol. 47, pp. 2040–2050, 2007.

[8] J. Vaithilingam, R. D. Goodridge, R. J. M. Hague, S. D. R. Christie, and S. Edmondson, "The effect of laser remelting on the surface chemistry of Ti6al4V components fabricated by selective laser melting," *Journal of Materials Processing Technology*, vol. 232, pp. 1–8, 2016.

[9] E. Łyczkowska, P. Szymczyk, B. Dybała, and E. Chlebus, "Chemical polishing of scaffolds made of Ti–6Al–7Nb alloy by additive manufacturing," *Archives of Civil and Mechanical Engineering*, vol. 14, no. 4, pp. 586–594, 2014.

[10] G. Pyka, A. Burakowski, G. Kerckhofs, M. Moesen, S. Van Bael, J. Schrooten, and M. Wevers, "Surface modification of Ti6Al4V open porous structures produced by additive manufacturing," *Advanced Engineering Materials*, vol. 14, no. 6, pp. 363–370, 2012.

[11] J. Kumar, "Ultrasonic Machining—a Comprehensive Review," *Machining Science and Technology*, vol. 17, no. 3, pp. 325–379, 2013.

[12] B. Pečnik, M. Hočevar, B. Širok, and B. Bizjan, "Scale deposit removal by means of ultrasonic cavitation," *Wear*, vol. 356–357, pp. 45–52, 2016.

[13] I. Tzanakis, D. G. Eskin, A. Georgoulas, and D. K. Fytanidis, “Incubation pit analysis and calculation of the hydrodynamic impact pressure from the implosion of an acoustic cavitation bubble,” *Ultrasonics Sonochemistry*, vol. 21, no. 2, pp. 866–878, 2014.
[14] C. Haosheng, W. Jiadao, and C. Darong, “Cavitation damages on solid surfaces in suspensions containing spherical and irregular microparticles,” *Wear*, vol. 266, no. 1–2, pp. 345–348, 2009.
[15] J. R. Laguna-Camacho, R. Lewis, M. Vite-Torres, and J. V. Méndez-Méndez, “A study of cavitation erosion on engineering materials,” *Wear*, vol. 301, no. 1–2, pp. 467–476, 2013.
[16] G. Strano, L. Hao, R. M. Everson, and K. E. Evans, “Surface roughness analysis, modelling and prediction in selective laser melting,” *Journal of Materials Processing Technology*, vol. 213, no. 4, pp. 589–597, 2013.
[17] P. P. Gohil and R. P. Saini, “Coalesced effect of cavitation and silt erosion in hydro turbines - A review,” *Renewable and Sustainable Energy Reviews*, vol. 33, pp. 280–289, 2014.
[18] Y. Ichida, R. Sato, Y. Morimoto, and K. Kobayashi, “Material removal mechanisms in non-contact ultrasonic abrasive machining,” *Wear*, vol. 258, no. 1–4 SPEC. ISS., pp. 107–114, 2005.
[19] J. Qu, A. Shih, R. Scattergood, and J. Luo, “Abrasive micro-blasting to improve surface integrity of electrical discharge machined WC–Co composite,” *Journal of Materials Processing Technology*, vol. 166, no. 3, pp. 440–448, 2005.
[20] L. Ventola, F. Robotti, M. Dialameh, F. Calignano, D. Manfredi, E. Chiavazzo, and P. Asinari, “Rough surfaces with enhanced heat transfer for electronics cooling by direct metal laser sintering,” *International Journal of Heat and Mass Transfer*, vol. 75, pp. 58–74, 2014.